Matter

CellPress

Article

Macro-superlubric triboelectric nanogenerator based on tribovoltaic effect

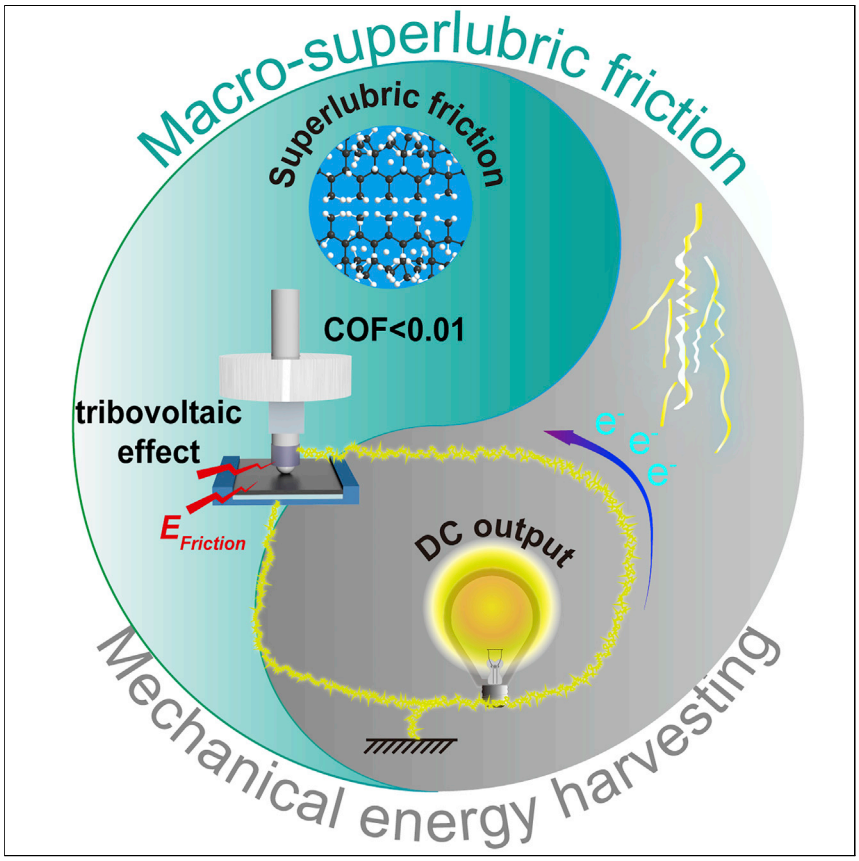

Liqiang Zhang, Haifang Cai, Liang Xu, ..., Feng Zhou, Weimin Liu, Zhong Lin Wang

wangda@licp.cas.cn (D.W.)
yfguo@nuaa.edu.cn (Y.G.)
wlguo@nuaa.edu.cn (W.G.)
zlwang@gatech.edu (Z.L.W.)

Highlights

A superlubric triboelectric nanogenerator (SL-TENG) in the macroscale is devised

The tribovoltaic effect causes the SL-TENG to have a direct current output

Enabled utilization of mechanical energy in the macro-superlubric friction state

Suitable for sensitive online friction state detection based on the unipolar output

Herein, a macro-superlubric triboelectric nanogenerator with ultralow friction coefficient (<0.01) and ultralow wear rate is reported for optimizing the performance of triboelectric nanogenerators, which output a direct-current electrical signal due to the tribovoltaic effect. This work addressed the lubrication problem of nanotriboelectric generators under high contact stress. Several LEDs can be illuminated without rectification via the unipolar electricity. The close relationship between friction and triboelectricity allows for the online monitoring and early warning of friction state.

6 **Development**
Practical, real world, technological considerations and constraints

Zhang et al., Matter 5, 1–15
May 4, 2022
https://doi.org/10.1016/j.matt.2022.02.021

Please cite this article in press as: Zhang et al., Macro-superlubric triboelectric nanogenerator based on tribovoltaic effect, Matter (2022), https://doi.org/10.1016/j.matt.2022.02.021

Matter

CellPress

Article

Macro-superlubric triboelectric nanogenerator based on tribovoltaic effect

Liqiang Zhang,[1,6] Haifang Cai,[2,6] Liang Xu,[3,6] Li Ji,[1] Daoai Wang,[1,4,7,*] Youbin Zheng,[1,4] Yange Feng,[1,4] Xudong Sui,[1] Yufeng Guo,[2,*] Wanlin Guo,[2,*] Feng Zhou,[1] Weimin Liu,[1] and Zhong Lin Wang[3,5,*]

SUMMARY

Reducing the coefficient of friction (COF) and wear rate is significant for triboelectric nanogenerators (TENGs). Here, we devised a new macroscale superlubric triboelectric nanogenerator (SL-TENG) that can withstand high-contact stress with ultralow COF (<0.01) and ultralow wear rate based on a hydrogenated diamond-like carbon (DLC) film from the tribological perspective. Specifically, the SL-TENG produced an output with the peak short-circuit current of approximately 60 nA and a power density of up to 5.815 W/m^2 during the friction of *DLC* versus *steel ball* with a Hertz contact stress of 1.37 GPa. Moreover, first-principle calculations demonstrate that the ultralow friction on DLC is mainly due to the hydrogen-terminated surface. The SL-TENG can generate direct current (DC) output caused by tribovoltaic effect and can light up several light-emitting diodes (LEDs) without rectification. Online superlubric friction monitoring and early warning can be realized, owing to the close correspondence between tribology and triboelectricity.

INTRODUCTION

Triboelectric nanogenerator (TENG), a new energy-harvesting technology based on the mechanism of triboelectrification and electrostatic induction, has attracted great attention in recent years.[1–6] Furthermore, this technology can conveniently collect disordered energy from friction processes or other mechanical processes and be widely used in energy supply, self-powered microelectronic devices, and sensors.[7–14] However, the frictional wear and long-term stability of TENG are also affected by the friction and wear condition of friction pair materials, which is the key for the practical application of TENGs to collect energy from interfacial friction. During the continuous contact-separation motion or long-term shear process, the friction pair materials, especially polymer-based friction layers, will inevitably wear and lead to decreased TENG energy collection efficiency and short working life. The severe wear behavior can even cause the friction layer to grind through and cause a short circuit of the electrodes, which is a disaster for TENG. Hence, the problem of wear during long-term friction process should be first solved to ensure that the TENG can efficiently work for a long time. Using materials with macroscale superlubricity to design a superlubric TENG (SL-TENG) with an ultralow coefficient of friction (COF) and wear rate is an effective solution.

Long-life working designs, such as changing the sliding friction to rolling friction, and some special designs about the noncontact rotary structure, the intermediate layer structure, the soft-hard contact TENG, and the slippery surface are critically important to TENG.[4,15–18] Recently, Professor Zheng's team first achieved the operation of

Progress and potential

Reducing the friction coefficient and solving the life problems caused by wear of macroscale triboelectric nanogenerators (TENGs) are necessary for the construction of long-service energy-harvesting devices. The high friction coefficient and wear rate of the current energy-harvesting devices are not conducive to the development of TENGs. This work provides an original fabrication strategy of a novel macro-superlubric triboelectric nanogenerator named "SL-TENG" based on tribovoltaic effect that is suitable for mechanical-energy harvesting and online friction-state detection. Compared with other materials, SL-TENG has a lower coefficient of friction (COF < 0.01) and wear rate and higher DC output under continuous friction process, paving the way for TENG's anti-friction and wear-resistant design.

Please cite this article in press as: Zhang et al., Macro-superlubric triboelectric nanogenerator based on tribovoltaic effect, Matter (2022), https://doi.org/10.1016/j.matt.2022.02.021

the structural Schottky superlubric generator in microscale, which proves the feasibility of the electrical output in the superlubricity.[19] However, the design of superlubricity of TENG in macroscale is still a challenge because friction pairs are limited by the mechanical interlocking, adhesion, and surface interaction in reality. In particular, many macroscopic friction processes in ball-on-flat contact are carried out at high speed and high normal load and need to withstand high contact stress, which faces tribological challenges. Interestingly, the current design of some carbon materials provides the possibility of achieving SL-TENG, especially the huge potential of macroscale superlubricity in the future.[20–25] Macroscopic TENGs based on tribovoltaic effect have received extensive attention. This kind of generator can directly output a direct current (DC) signal, which is expected to realize the direct utilization of interface energy without rectification. However, its friction pair materials are mainly semiconductors (such as Si), which have problems, such as brittleness, poor wear resistance, and short life. Therefore, there is an urgent need to apply antiwear materials to solve the tribological problem in the tribovoltaic effect. Hydrogenated diamond-like carbon (DLC) films, which are excellent solid-lubricating materials with good wear resistance, have low COF (COF < 0.01) under high normal load and high-frequency friction conditions, even in a high vacuum environment or inert atmosphere.[26–28] Based on the inherent close relationship between triboelectricity and friction, the electric energy collection system combined with friction can also be used to design an *in situ* sensor to monitor the friction state, which is important and meaningful in practical applications.[26–29]

Herein, a new type of macroscale SL-TENG was fabricated based on the hydrogenated DLC coating in the continuous friction process for mechanical-energy harvesting and friction-state detection. In the macroscopic ball-on-disk contact mode, SL-TENG has achieved a current of 60 nA and power density of up to 5.815 W/m^2. Moreover, SL-TENG has an extremely low COF of less than 0.01 and a low wear rate compared with sliding triboelectric generators with the friction pair of graphite-like carbon (GLC) film and polytetrafluoroethylene (PTFE). Thus, SL-TENG has a long working life and a high energy-harvesting efficiency under high load and high-speed friction conditions. The current analysis of the friction process and the first-principle calculations indicated that the ultralow friction of SL-TENG is mainly attributed to the low energy barrier between the hydrogen-terminated surfaces. In addition, the DC output is attributed to the tribovoltaic of the rubbing interface. The situation as mentioned above effectively ensures the realization of high triboelectric energy harvesting under superlubric friction in macroscale. A method of online detection of superlubric friction state failure by friction electrification is proposed on the basis of the inseparable relationship between triboelectricity and the COF of the SL-TENG. This method shows the tremendous potential of real-time friction state detection in the actual closed working condition.

RESULTS

Fabrication of the macroscale SL-TENG

Figures 1A and 1B show the preparation process, molecular structure, and the atomic force microscopic (AFM) image of the hydrogen-containing DLC film, which was fabricated by a magnetron sputtering method with the composition of a network of sp^2 carbon atoms, sp^3 carbon atoms, and hydrogen atoms.[30,31] The surface of the prepared DLC film has a nanometer-scale roughness of 1.03 nm, which is beneficial for reducing the mechanical interlocking of microstructures during friction.[32] The hydrogenated DLC films have low COF under high normal load and high-frequency friction conditions, even in a low vacuum environment. This situation is due to the following: the weak mechanical interlocking of the smooth surfaces and the low

[1]State Key Laboratory of Solid Lubrication, Lanzhou Institute of Chemical Physics, Chinese Academy of Sciences, Lanzhou 730000, China

[2]State Key Laboratory of Mechanics and Control of Mechanical Structures and MOE Key Laboratory for Intelligent Nano Materials and Devices, College of Aerospace Engineering, Nanjing University of Aeronautics and Astronautics, Nanjing 210016, China

[3]Beijing Institute of Nanoenergy and Nanosystems, Chinese Academy of Sciences, Beijing 101400, China

[4]Qingdao Center of Resource Chemistry and New Materials, Qingdao 266100, China

[5]School of Materials Science and Engineering, Georgia Institute of Technology, Atlanta, GA 30332-0245, USA

[6]These authors contributed equally

[7]Lead contact

*Correspondence: wangda@licp.cas.cn (D.W.), yfguo@nuaa.edu.cn (Y.G.), wlguo@nuaa.edu.cn (W.G.), zlwang@gatech.edu (Z.L.W.)

https://doi.org/10.1016/j.matt.2022.02.021

Please cite this article in press as: Zhang et al., Macro-superlubric triboelectric nanogenerator based on tribovoltaic effect, Matter (2022), https://doi.org/10.1016/j.matt.2022.02.021

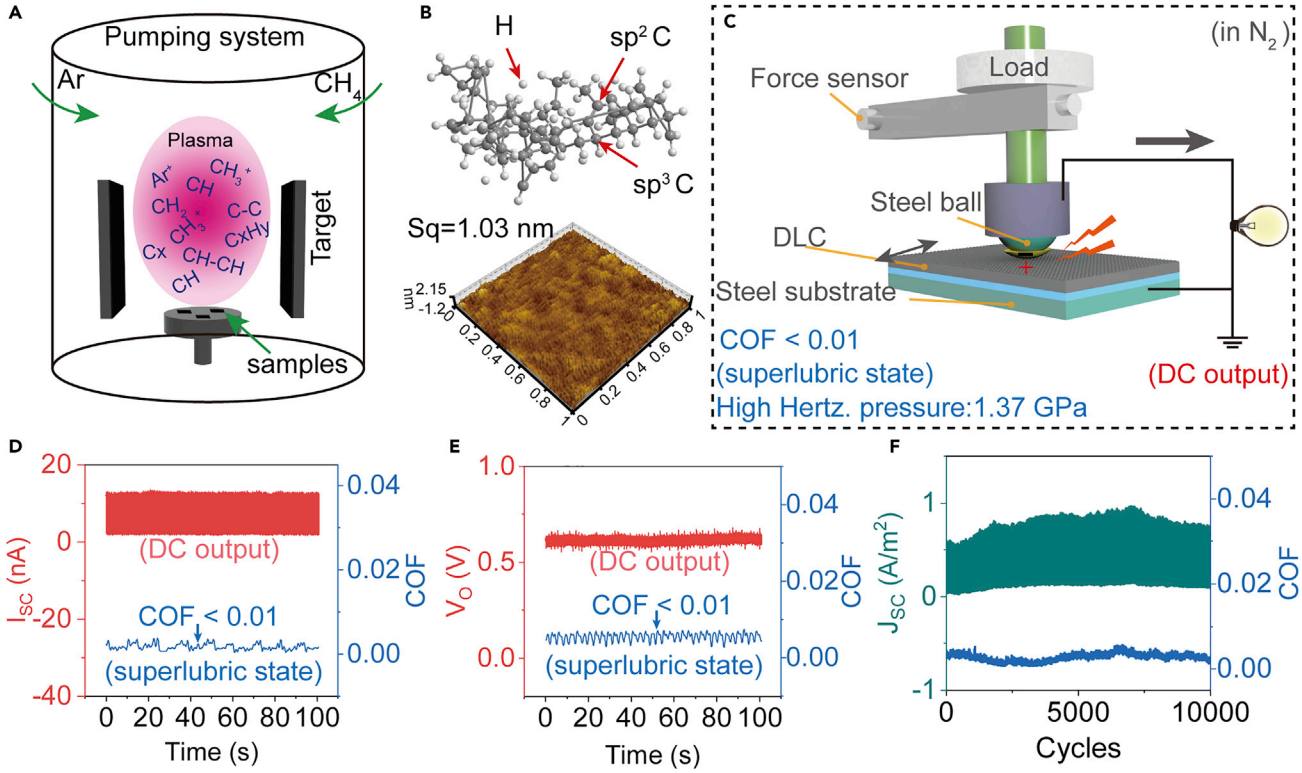

Figure 1. Concept display and schematic diagram of the macroscopic SL-TENG

(A) Schematic illustration of the preparation of the hydrogen-containing DLC film.

(B) Molecular structure and AFM image of the DLC film.

(C) Schematic of the fabrication of the SL-TENG based on a ball-on-disc friction mode with DLC film and steel ball as the friction pair.

(D) I_{SC} and its corresponding COF of the SL-TENG. The friction is carried out under a load of 10 N (Hertz contact stress of 1.37 GPa), an amplitude of 5 mm, and a frequency of 6 Hz. The atmosphere is dry nitrogen (relative humidity [RH] < 10%).

(E) V_O and its corresponding COF of the SL-TENG. The friction is carried out under a load of 10 N (Hertz contact stress of 1.37 GPa), an amplitude of 5 mm, and a frequency of 6 Hz. The atmosphere is dry nitrogen (RH < 10%).

(F) J_{SC} of the SL-TENG in 10,000 cycles and the corresponding COF. The friction is carried out under a load of 10 N (Hertz contact stress of 1.37 GPa), an amplitude of 5 mm, and a frequency of 6 Hz. The atmosphere is dry nitrogen (RH < 10%).

interfacial adhesion caused by the formation of the transfer film, the low σ bond content of the DLC film, the weakened π–π* interaction, and the high passivation of the carbon–hydrogen bond to the surface.[26,27,33] This notion means that the work conducted by the mechanical friction motion is rarely dissipated by thermal energy or adhesive wear, but it is converted into other forms of energy, such as electricity; thus, the DLC film has a greater potential to improve its frictional energy conversion efficiency than the ordinary polymers and is more promising for use in sliding-mode TENGs.[34,35]

The friction pairs, DLC film and steel ball, are assembled to be the SL-TENG to simultaneously harvest the triboelectric energy during the friction process and explore the relationship between triboelectricity and tribological behavior of friction pairs *in situ*. A commercial friction-testing machine directly drives the above-mentioned pairs to realize the superlubric friction motion with a ball-on-disc friction mode in an inert nitrogen atmosphere (Figure 1C). The steel ball fixture consists of an insulated rod and a conductive holder to avoid the electromagnetic interference from the machine. In this designed SL-TENG system, the steel ball was a rubbing surface and acted as an electrode connected to the ground wire and the steel backplane of the DLC via the

Please cite this article in press as: Zhang et al., Macro-superlubric triboelectric nanogenerator based on tribovoltaic effect, Matter (2022), https://doi.org/10.1016/j.matt.2022.02.021

load. On the one hand, the electric information of SL-TENG was collected through the external electrical test devices during the superlubric process. On the other hand, the COF was collected by the built-in sensor of the friction-testing machine. Therefore, the triboelectric and COF can be simultaneously collected to analyze the behavior of triboelectricity during the friction process. Herein, superlubricity in the macroscale (COF < 0.01) and DC output are two main features of SL-TENG during the reciprocating or rotational friction process.

The short-circuit current (I_{SC}) and output voltage (V_O) of the SL-TENG based on ball-on-disk reciprocating friction mode are presented in Figures 1D and 1E, respectively. The COF can reach from 0.002 to 0.009, which is considered to be superlubricity.[36,37] Under this superlubric friction condition, the I_{SC} and V_O can reach a peak value of approximately 16 nA and 0.6 V, respectively. The electrical signals obtained during the superlubric friction stage are both DC unipolar positive, different from the normal TENGs with alternating current. In addition, the increase in load and maximum speed will enhance the output of triboelectricity (Figure S1). Figure 1F shows that the current density (J_{SC}) of SL-TENG can reach more than 0.7 A/m^2, and it is relatively stable during 10,000 reciprocating cycles under a COF that is below 0.01. The maximum measured voltage is also maintained at approximately 0.5 V, and a power density of 0.47 W/m^2 can be achieved in the case of this reciprocating friction (Figure S2).

Advantages of SL-TENG

Figure 2A displayed the evolution of the triboelectricity and COF during the entire friction process in the 1st hour to understand the formation of triboelectricity in a macro-superlubric friction state. During the entire friction process, the I_{SC} of SL-TENG has undergone a transition from a negative peak shape to a positive peak shape. At the initial stage (Figure 2A-I), the COF rapidly increased. The surfaces of the steel ball and DLC film are severely worn, corresponding to the increase in the absolute value of the I_{SC}. After that, the I_{SC} continues to increase negatively (Figure 2A-II). The DLC film may gradually transfer to the steel ball in this stage due to the interface adhesion. Moreover, the low adhesion between the transfer film on the surface of the steel ball and the DLC substrate greatly reduced the interaction between the rubbing interfaces. The COF is still greater than 0.01.

Thereafter, the amplitude of the I_{SC} decreases gradually (Figure 2A-III). This phenomenon is probably caused by the formation of material transfer (the material transfer results in two surfaces of similar properties). In other words, the work functions of the friction pair are gradually approaching. Afterward, the polarity of the I_{SC} reversed (Figure 2A-IV). Before and after stage IV, the COF of SL-TENG has been less than 0.01. When the polarity of the current is reversed, SL-TENG first undergoes a positive I_{SC} increase process (Figure 2A-V). Finally, SL-TENG enters the stage of dynamically steady electricity harvesting with superlubricity (Figure 2A-VI). Consequently, the friction process can be divided into three stages according to the polarity division of the I_{SC}: the running-in stage, the stage of polarity inversion, and the dynamic stable superlubric stage (Figure S3). After the friction in the superlubric friction stage, the depth and width (Figure S4) of the wear scar did not become deep and wide. Therefore, the superlubric stage is almost at the zero-wearing state and has a great potential of long-time, low-wear operation. In addition, the surface potential test also shows a similar evolution process of polarity reversion (Figure S5).

The carbon transfer film will adhere to the surface of the steel ball during the friction process. Figures 2B and 2C display the scanning electron microscope (SEM) image

Please cite this article in press as: Zhang et al., Macro-superlubric triboelectric nanogenerator based on tribovoltaic effect, Matter (2022), https://doi.org/10.1016/j.matt.2022.02.021

CellPress

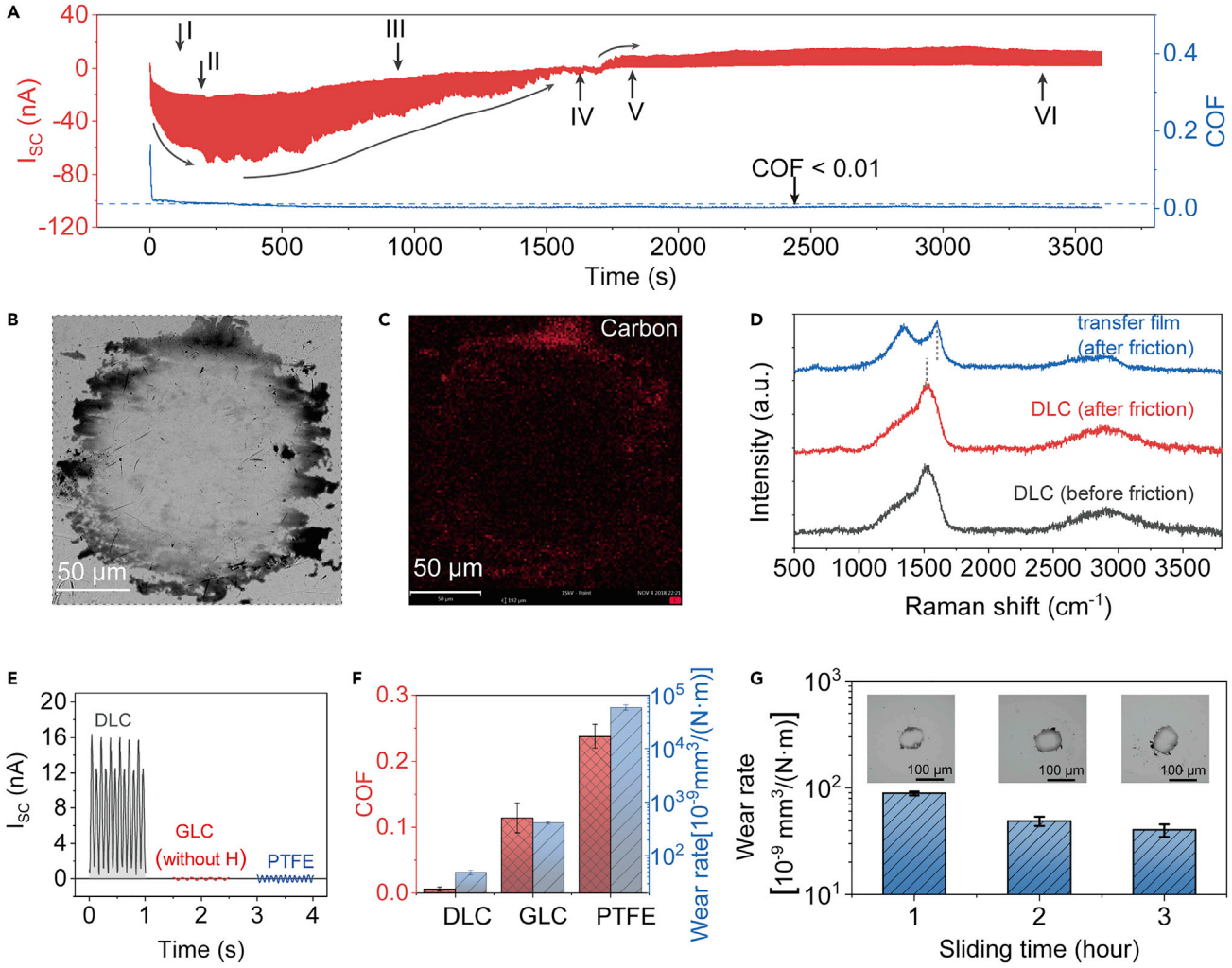

Figure 2. The great advantages of DLC-based SL-TENG

(A) Comparison of the whole curve of I_{SC} and COF of the SL-TENG. The friction is carried out under a load of 10 N, an amplitude of 5 mm, and a frequency of 6 Hz. The atmosphere is dry nitrogen (RH < 10%).

(B) The scanned electron microscopic image of the transfer film adhered to the surface of the steel ball. Scale bar, 50 μm.

(C) The corresponding carbon element EDS distribution map.Scale bar, 50 μm.

(D) Raman spectra of the transfer film and DLC film before and after the friction process.

(E and F) I_{SC}, COF, and the wear rate of SL-TENG when steel ball rubbed with the DLC film, GLC film, and PTFE. The data in (E) were presented as mean ± SD and sample size n = 3.

(G) Wear rate after the friction between the steel ball and the DLC for 1, 2, and 3 h. The inset images are the wear surfaces of the GCr15 steel ball at different frictional times.Scale bar, 100 μm. The data in (G) were presented as mean ± SD and sample size n = 3.

and corresponding energy dispersive X-ray spectroscopy (EDS) image of the transfer film adhered to the steel ball. The Raman spectra (Figure 2D) of the transfer film adhered on the surface of the steel ball show a characteristic peak of the amorphous structure of carbon.[38] The G peak of the transfer film tends to shift toward a high-frequency region, thereby indicating that the structure of the transfer film changed to graphitization.[39–43]

The currents of the GLC film and PTFE under the same frictional conditions were used for comparison to further understand the huge advantages of SL-TENG in terms of triboelectricity and friction. Figure 2E shows that the I_{SC} values are approximately 0.5 and 1 nA when the steel ball is rubbed with the GLC film and PTFE under

Please cite this article in press as: Zhang et al., Macro-superlubric triboelectric nanogenerator based on tribovoltaic effect, Matter (2022), https://doi.org/10.1016/j.matt.2022.02.021

the same conditions. The I_{SC} during the entire frictional process of the steel ball with GLC film and PTFE is shown in Figure S6. The I_{SC} of the SL-TENG is more than 10 times that of the GLC film or PTFE. Meanwhile, the I_{SC} of the SL-TENG shows a unipolar peak shape that is different from other materials. The working principle of TENG composed of PTFE and GLC is discussed in Figure S7.

Figure 2F shows that the DLC film has a lower COF and wear rate than those of the GLC film and PTFE during the stable friction process. The average COFs of GLC and PTFE are 0.11 and 0.24, which are 18 and 40 times of DLC, respectively. In addition, the wear rates of GLC and PTFE are 8 and 1,235 times those of DLC, respectively. Figure S8A demonstrates that the 3D wear scar images of the three materials intuitively show the excellent wear resistance of DLC. Figure S8B exhibits that the wear depth of the DLC film is 0.28 μm, while those of GLC and PTFE are 1.4 and 40 μm, respectively. This finding indicates that the DLC film is an attractive material with superior tribology and electrical properties under this continuous friction condition. In other words, we solve the problem of high friction and wear under high-contact-stress state by selecting materials rather than improving friction conditions, which has more important application potential in engineering. Figure 2G shows that, after the DLC film has undergone a friction process of 1, 2, and 3 h, the wear rate did not drastically change, thereby indicating its long-term operating life. The inset SEM image of the surface of the GCr15 steel ball paired with the DLC film also proved that the wear area remained basically constant. The 3D image and the wear depth of the wear scar in Figures S7C and S7D show that it will not cause serious wear with time.

Working principle of the SL-TENG

Triboelectrification caused by continuous sliding friction of the components during actual mechanical movement is common. In the conventional TENG, the two friction layers have separation processes of overlapped charged surfaces, and the potential difference between the electrodes drives the free electrons to flow in the external circuit (Figure S9A). The situation is different here. The friction area of the steel ball or other friction pairs is always in contact with the underlying substrate during the friction process in the industrial machinery (Figure S9B). Herein, the DC triboelectricity signal may be attributed to the tribovoltaic effect based on the heterojunction interface (Figure 3A).[44–46] Once a metal slides on a semiconductor surface, the instantaneously newly formed atomic bond at the interface would release an energy quantum, named as "bindington," which excites electron-hole pairs at the interface. The electrons and holes are separated by the Schottky barrier at the interface, resulting in a direct current. This is the tribovoltaic effect for the metal-semiconductor case. As shown in Figure S10A, we confirmed that the prepared DLC should have a semiconductor property through a test of the photovoltaic effect. When a bias voltage is applied to the surface of the DLC, with the irradiation of 365 nm UV light, the current through the DLC exhibits a significant increase (Figure S10B), and the current gradually returns to the original level after closing the UV source. The result proves that the prepared DLC has characteristics of semiconductor because photoelectrons are challenging to be excited for the insulator. Moreover, as shown in Figures S10C and S10D, the scanning current-voltage characteristic curve (I-V curve) further confirms the semiconductor property of prepared DLC.

Figure 3B depicts the energy band diagram when the work function of steel ball is lower than that of DLC ($W_{Fe} < W_{DLC}$). In the initial noncontact state (1), the steel ball and DLC constitute a friction pair and their work functions are different. The work function of samples is tested through a contact-less measurement using Kelvin probe with a reference gold tip. The measured work function of steel is about 4.63

Please cite this article in press as: Zhang et al., Macro-superlubric triboelectric nanogenerator based on tribovoltaic effect, Matter (2022), https://doi.org/10.1016/j.matt.2022.02.021

CellPress

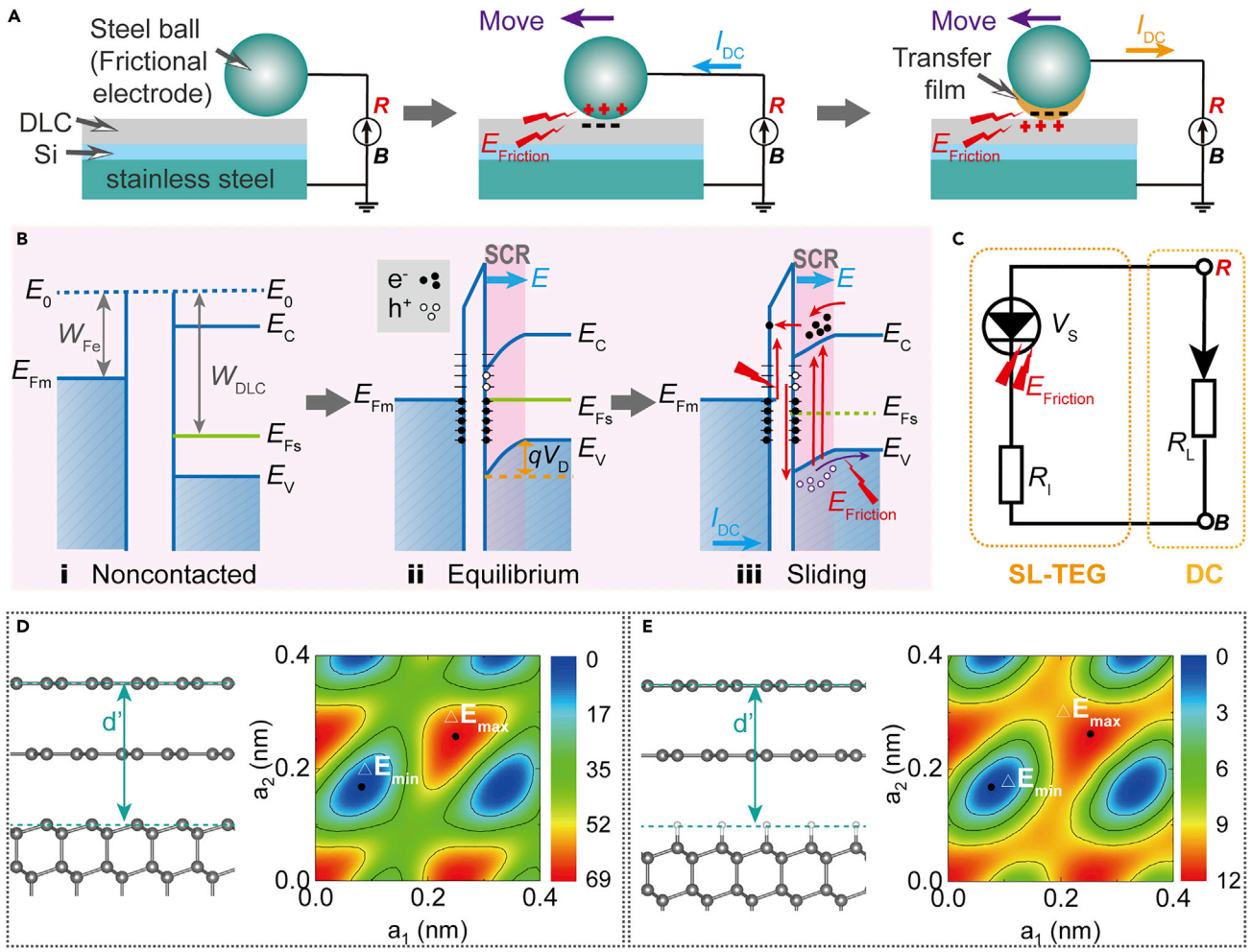

Figure 3. Proposed working principle of the SL-TENG

(A) Composition of friction interface during the friction process. "R" and "B" represent the connection modes.

(B) Energy band diagram of the MS junction in the noncontact state, equilibrium state, and sliding state.

(C) Equivalent circuit diagram of the SL-TENG.

(D and E) Side views of atomic configurations and the corresponding PESs (in unit of meV per unit cell) for surface dangling bonded and H-terminated diamond slabs with an sp2 hybridized graphite bilayer under an interlayer distance d' of 0.60 nm. The gray and white balls represent carbon and hydrogen atoms, respectively. The dots denote the positions when the relative movement of graphite bilayer and diamond slab reaches the highest energy state ΔE_{max} and the lowest energy state ΔE_{min}.

eV, and the work function of DLC is about 4.85 eV (Figure S11). In the second state (2), the friction pair is in good contact under the pressure of the load. Due to the difference of the Fermi level (E_F), the electrons will flow from the steel ball side to the DLC side to establish a state of equilibrium, accompanying the energy band of DLC to be bent downward, and form the built-in electric field at the space charge region (SCR) on the DLC side. There are two ways for exciting charge carriers under friction.[47] On the one hand, the electron-hole pair under frictional excitation will drift under the influence of the built-in electric field. For example, the electrons will drift to the metal side under the influence of the built-in electric field. On the other hand, some electrons at the surface state will jump to a higher energy level under the excitation of friction, overcoming the potential barrier at the junction interface. The holes may also be excited similarly. Thus, due to the tribovoltaic effect, a potential difference (V_S) will be formed and a direct current flow in the external circuit will be tested

Please cite this article in press as: Zhang et al., Macro-superlubric triboelectric nanogenerator based on tribovoltaic effect, Matter (2022), https://doi.org/10.1016/j.matt.2022.02.021

during the sliding process.[47–49] Figure 3C depicts the equivalent circuit diagram of the SL-TENG based on the above theory.[47] The friction part can be simplified as a friction-induced generation diode (V_S) and an internal resistance (R_i). The mass spectrometry (MS) interface will produce a DC output for the external load (R_L) under the action of the friction. The working mechanism after forming the transfer film can be deduced similarly.

On the nanometer scale, the hydrocarbon suspension bonds and the formation of transfer layers also have important contributions to reducing frictional resistance.[32] The effect of transfer film and hydrogen sealing on the frictional energy of the interface during the friction process has been studied by first-principle calculations on density-functional theory (DFT). In our model, a (111) diamond slab is established in the rhombus unit cell ($a_1 = a_2 = 2.514$ Å) to represent the DLC film, which consists of eight layers and eight carbon atoms. The bottom surface of the diamond slab is passivated by hydrogen atoms. A graphite bilayer is placed on the diamond slab to simulate the sp^2 hybridized carbon transfer layer. The interface of the diamond slab is in dangling bond (Figure 3D) state or H terminated (Figure 3E). All computations are performed within the framework of DFT as implemented in the Vienna Ab initio Simulation Package (VASP) code by using the projector augmented wave method with the Perdew-Burke-Ernzerhof (PBE) exchange-correlation functional,[50–52] and the plane wave energy cutoff is set to 500 eV. The influence of van der Waals (vdW) interactions is considered by using a modified version of vdW-DF, referred to as "optB86b-vdW." The PBE exchange functional of the original vdW-DF is replaced with the optB86b exchange functional to yield accurate equilibrium interatomic distances and energies for a wide range of systems.[53,54] A vacuum thickness of over 15 Å is set in the perpendicular direction to avoid an interaction from the periodic boundary condition. The whole system is relaxed by using a conjugate-gradient algorithm until the force on each atom is less than 0.1 eV/nm. In all relaxation processes, special k points sampled on a 10 × 10 × 1 mesh are employed. After geometric optimization, the top graphite bilayer is transversely moved with respect to the underlying diamond slab and relatively slides to different positions and the whole system is relaxed again. During the sliding processes, the distance between the top layer of graphite and the surface layer of diamond slab with or without H termination is fixed at a constant interlayer distance. After structural relaxation, a higher k point density sampled on a 20 × 20 × 1 mesh is employed to calculate the total energy at different sliding positions. The corresponding potential energy surfaces (PESs) for interlayer sliding are constructed by the difference between the total energy E and the minimum total energy E_{min} of the system $\Delta E = E - E_{min}$ when the graphite bilayer slides to different positions. Furthermore, Figures 3D and 3E show the PESs of in-plane interlayer sliding of the graphite bilayer on the diamond slab at a constant interlayer distance d' of 0.6 nm. The maximum sliding energy corrugation ($\Delta E_{max} - \Delta E_{min}$) of the H-terminated state is much lower than that of the dangling bond state, thereby indicating a low interface sliding resistance.[55,56] The friction reduction at the H-terminated interface is consistent with the experimental measurement.

Applications of SL-TENG

SL-TENG can be applied in both energy harvesting and friction-state sensing. At present, most of the DC-TENGs based on the tribovoltaic effect are mostly based on the flat-on-flat friction mode, while the motion mode of ball-on-flat friction motion is limited in practical applications due to severe wear and high friction coefficient. We coupled the DLC into the research system of the tribovoltaic effect and realized the electric energy harvesting in the ball-on-flat mode. An application of

Please cite this article in press as: Zhang et al., Macro-superlubric triboelectric nanogenerator based on tribovoltaic effect, Matter (2022), https://doi.org/10.1016/j.matt.2022.02.021

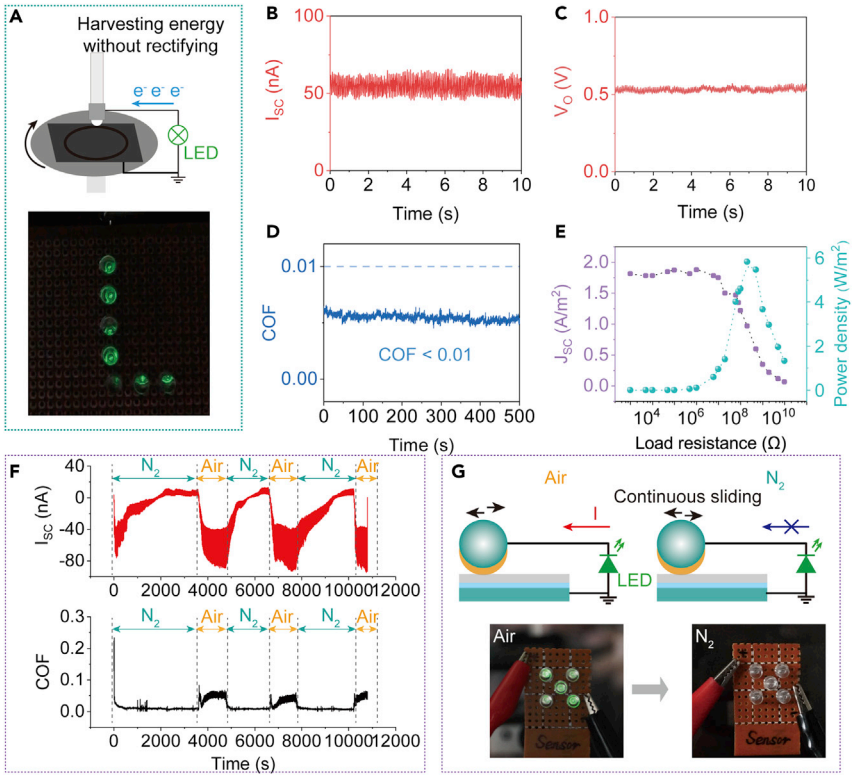

Figure 4. Mechanical energy harvesting of SL-TENG and its application of friction-state monitoring

(A) Schematic of the energy-harvesting system based on the rotation mode, and the optical picture shows that seven LEDs connected in series are illuminated. The friction was carried out under dry nitrogen at a linear speed of 50 cm/s and a load of 10 N.

(B–D) I_{SC} (B), V_O (C), and COF (D) of SL-TENG in the rotation friction mode.

(E) Comparison of J_{SC} and the power density of SL-TENG.

(F) I_{SC} curve collected with a current amplifier and its corresponding COF curve under different atmospheric changes.

(G) A circuit for sensing the failure of superlubric friction by using the unipolarity of the current and the corresponding optical photo of the LED lamp when nitrogen and oxygen are injected.

the triboelectric energy harvesting based on the rotation mode was demonstrated to show the feasibility of energy harvesting at the friction interface of SL-TENG. Figure 4A shows that, during the stable friction process, electrons flow from the ground into the upper friction interface; thus, the positive electrode of the LED is connected to the steel ball, and the negative pole of the LED is connected to the steel plate of DLC and the ground line. In this mode, the energy collected from the friction interface can be directly used without rectification and several green LEDs can be directly and continuously lighted (Video S1). Figures 4B and 4C show that the correlational peak I_{SC} and peak V_O at this time can reach 60 nA and 0.55 V, respectively. Figure 4D presents that the stable COF in the rotating mode is approximately 0.006. In this case, the J_{SC} can reach values as high as 1.7 A/m^2; in addition, SL-TENG's DC output is more advantageous than traditional TENG (Figure S12). The results of the comparison of J_{SC} and the power density of SL-TENG are presented in Figure 4E. The J_{SC} of SL-TENG decreases with the increase in the load resistance, and the power density of SL-TENG reaches 5.815 W/m^2 when the load resistance is 200 MΩ. This remarkable high output means the advantage of superlubric energy harvesting in the future.

Please cite this article in press as: Zhang et al., Macro-superlubric triboelectric nanogenerator based on tribovoltaic effect, Matter (2022), https://doi.org/10.1016/j.matt.2022.02.021

In many cases, the information in the friction process reflected by the friction force curve is too little to reflect the friction state of the friction pair well. Thus, real-time sensing of the friction state is extremely important in tribology, which is helpful for us to understand the state of the friction pair and ensure the normal operation of the friction. Therefore, it is necessary to combine other test methods to characterize the friction interface state globally. The triboelectric signal is closely related to the friction state. Using the change of the electric signal to monitor the friction state is a very suitable and important means in friction sensing. The friction state *in situ* during the actual sliding should be grasped to maintain the safe operation of the machine and handle possible failures. Superlubric friction at macroscale is undoubtedly significant for the life of the TENGs, and the failure of the superlubricity will greatly reduce its service life. However, some abnormal accidental factors may negatively influence the use of DLC film in the actual application. Thus, detecting the failure of the material's superlubric friction state is critical. This method effectively detects the abnormal tribological conditions between the steel ball and the DLC film due to the good correspondence relation between the COF and the I_{SC}. Figure 4F demonstrates that the COF and I_{SC} of the SL-TENG will closely change with the intermittent injection of nitrogen and air. A positive current of approximately 14 nA was collected while under a dry inert nitrogen atmosphere. The corresponding COF was below 0.01. When ambient air is injected, the current in the steady stage reached −80 nA, and the COF also rose to approximately 0.05. The DLC film has experienced severe wear in the air (Figures S13A and S13B). In addition, the design of DC-TENG with high current output occupies a very important position in the engineering application of TENG in the future. Although the superlubric friction state of SL-TENG fails in air, the current output in air is really large and its friction coefficient is relatively low (COF < 0.1) compared with conventional polymers. Thus, the DLC can also be designed as a low-friction DC-TENG in the range of conventional lubrication. If the atmosphere was repeatedly changed, then the friction current would change with the modification of the COF, and this repetition process is sensitive. This situation allows the current in the friction process to be used to detect the friction state *in situ*. The change of the atmosphere can be visually detected by illuminating the LED by a simple circuit (Figure 4G) without rectification. When rubbing in the atmospheric environment, the system generates a negative current signal, and the excited electrons flow into the negative pin of the LED connected to the steel ball to light it. While in the nitrogen environment, the LED light cannot be lit up. Therefore, we use the characteristics of different current output polarities to connect the unidirectional output LEDs to the circuit so that it can only be turned on in the air, enabling *in situ* monitoring of superlubricity failure caused by transition from nitrogen to air. Given that the superlubric current in nitrogen is positive, the LEDs cannot be illuminated because it only allows the current to flow in one direction. The current collected in the air was negative, which may be due to the heterojunction friction of steel ball and DLC. In addition, friction in the air is also accompanied by adsorption of water molecules, oxygen, etc. and the oxidation of the interface (Figure S13C).[57] Thus, the LEDs can be illuminated in the air. The change of LEDs when changing from nitrogen to air is shown in Video S2. In this way, we can realize the sensing of friction state on the basis of the unipolarity of the current.

The above method can even be used to sense other frictional conditions, such as when certain objects (e.g., oil and water) that have a negative influence on normal friction in the actual application are present at the interface. Figure S14A shows that, when some water is present at the rubbing interface, the friction coefficient will increase to approximately 0.15. The current at this time exhibits a polymer-like bidirectional current characteristic, and its value decreases. When some Poly Alpha Olefin

Please cite this article in press as: Zhang et al., Macro-superlubric triboelectric nanogenerator based on tribovoltaic effect, Matter (2022), https://doi.org/10.1016/j.matt.2022.02.021

(PAO) 10 base oil was present at the interface, the transfer film was isolated by the oil film and the friction coefficient increased to 0.08. Furthermore, the SL-TENG lost the characteristics of DC high output due to the failure of the frictional effect since the contact interface is separated by the insulating oil (Figure S14B). Consequently, these derived abnormal friction situations can also be monitored by triboelectric signals on the basis of the close relationship between triboelectricity and friction coefficient. Whether in the tribological test or in the actual friction monitoring in the future, the *in situ* self-powered monitoring of triboelectrification will have prominent applications.

In the research history of tribology, the classical tribological laws are summarized from the macroscopic friction motion, and the relationship between the load, friction coefficient, friction speed, etc. and friction force is approximately established. However, the classical tribological laws have great limitations and must be studied in depth. The energy dissipation mechanism of friction has always been the core issue of basic research in tribology. The energy dissipation at the microscopic level is the cause of the phenomena, such as heat, force, light, and electromagnetic radiation, in the macroscopic friction. Among them, triboelectric electrification is a common phenomenon in interfacial friction, in which electrons are continuously transferred, excited, and flowed between two surfaces. Most of the current research on the relationship between triboelectrification and friction force is based on contact resistance (friction between metal and metal), surface potential (mainly for dielectric), current and voltage to ground (friction involving metal friction pairs), and other test methods, ignoring the relationship between carrier transfer and friction at different interfaces that require different energy values for processes such as electron excitation. It is difficult to determine the necessary relationship between the tribovoltaic effect and friction because of many factors that influence friction. However, how to control friction by regulating the tribovoltaic effect is a possible research direction in the future.

DISCUSSION

In summary, we combined the tribology test machine with TENG on the basis of the continuous friction of the ball-on-disk contact mode with high contact stress. We also realized the collection and utilization of triboelectric energy in the state of macroscopic friction with superlubricity and solved the problem with the silicon-material-based DC-TENG with high COF and wear rate. During the macroscopic friction process with a COF of less than 0.01 and an ultralow wear rate, SL-TENG has a I_{SC} output about 60 nA and a J_{SC} output of up to 1.7 A/m^2, and its energy density can reach 5.815 W/m^2. The potential difference produced by friction provides a path for converting mechanical energy into electrical energy at macroscale. The first-principle calculations indicate that the ultralow friction on the DLC film is mainly attributed to the hydrogen-terminated surface. This design that closely combines COF and triboelectricity provides a new strategy for macroscopic energy harvesting and friction-state detection of mechanical motion, which has good prospects in the field of tribology and self-powered sensing. Furthermore, this work also provides a new research direction for the tribological design of heterogeneous friction interfaces.

EXPERIMENTAL PROCEDURES

Resource availability

Lead contact

Further information and requests for resources and reagents should be directed to and will be fulfilled by the lead contact, wangda@licp.cas.cn.

Please cite this article in press as: Zhang et al., Macro-superlubric triboelectric nanogenerator based on tribovoltaic effect, Matter (2022), https://doi.org/10.1016/j.matt.2022.02.021

Materials availability

This study did not generate new unique reagents. Steel ball (GCr15, Ningyang Xinxin Stainless Steel Ball Manufacturing), phosphorus pentoxide (Tianjin Kemiou Chemical Reagent), and PAO 10 oil (SpectraSyn 10, ExxonMobil (China) Investment) were used.

Data and code availability

All data needed to evaluate the conclusions in the paper are present in the paper and/or supplemental information. Any additional information required to reanalyze the data reported in this paper is available from the lead contact upon request.

Preparation of the hydrogenated DLC film

The hydrogenated DLC film with a thickness about 2.5 μm was deposited on a polished stainless-steel plate (φ50 mm × 30 mm, 1Cr18Ni9Ti) by the unbalanced magnetron sputtering method with the help of an external-field-induced growth effect of an a-C:H film, which used methane as a hydrogen source.[28,58] The nonhydrogenated GLC film was prepared by a similar method without the introduction of CH_4.

Preparation of SL-TENG

A steel ball (GCr15) with a diameter of 6 mm was simultaneously chosen as an electrode and the upper friction pair. First, the steel ball was fixed in a metal holder and insulated from the rest of the tribometer (TRB) (Anton paar). A copper wire was then stuck onto the surface of the metal holder in the lower part. The hydrogen-containing DLC film deposited on the stainless-steel plate was used as another friction layer of the SL-TENG. The steel plate was well grounded to avoid other electromagnetic interferences.

Fabrication of the friction-triboelectricity coupling test system

The tribometer was wrapped in aluminum foil, which was well grounded to avoid external electromagnetic interference. The relative humidity of the entire friction environment after drying by phosphorus pentoxide is less than 10%. When measuring the I_{SC}, the two input terminals of the current amplifier are respectively connected to the copper wire led from the steel ball holder and to the ground. The coefficient of friction, the I_{SC}, or the output voltage (V_O) from the friction process were synchronously collected when the friction pair is in contact and shearing. The superlubric friction process adopts a linear reciprocating mode in N_2 with a relative humidity less than 10%, an amplitude of 5 mm, a load of 10 N, and a reciprocated frequency of 6 Hz (9.4248 cm/s). When collecting energy in rotating mode, the friction process was carried out under dry nitrogen at a linear speed of 50 cm/s and a load of 10 N.

Characterization

The COF of the DLC film was obtained by the build-in force sensor of the tribometer. The 3D wear morphology and the wear rate were obtained with a 3D profile analyzer (Micro XAM 800). The AFM images were acquired using Agilent 5500 AFM (Agilent Technologies, USA) with a contact mode. The SEM images and elemental analysis images were acquired by Phenom ProX (Phenom, the Netherlands). The contact area between the steel ball and the DLC film was approximately 17,000 μm^2 measured from the wear scar area after testing. The contact area under stable friction was basically unchanged. The Raman spectra of the DLC film, the transfer film on the steel ball, and the GLC film were measured through the Raman spectroscopy (Horiba LabRam HR800) with a 532-nm wavelength excitation.

The collected I_{SC} was detected via the SR570 Low Noise Current Preamplifier (Stanford Research System, USA) with a filter frequency of 10 Hz (at this frequency,

ambient and machine noise is avoided and current is easier to identify under this filter). The short-circuit current density (J_{SC}) of SL-TENG was obtained by dividing the current by the contact area. The V_O of the SL-TENG was measured with a resistor of 100 MΩ in series. The surface potential was detected through electrostatic measuring probe (SK050 and SK1000, KEYENCE [China]) at a distance about 5 mm. The current and voltage data during the rubbing of the DLC film were collected via NI PCIe-6259 DAQ card (National Instruments, USA) and exported through a LabVIEW BASE Development System (National Instruments). In the test, A layer Cr is deposited as an electrode on the surface of the DLC surface (SuPro Instruments ISC150T, SuPro Instruments). The I-V curve is collected by Keithley 2400 Source Meter. The work function was tested through an atmospheric Kelvin probe in a Faraday cage (KVP-00-00-00, Instytut Fotonowy Poland).

SUPPLEMENTAL INFORMATION

Supplemental information can be found online at https://doi.org/10.1016/j.matt.2022.02.021.

ACKNOWLEDGMENTS

We gratefully acknowledge support from the NSFC (nos. U21A2046, 51905518, 11972186, 11890674, and 51921003), the Key Research Program of the Chinese Academy of Sciences (grant no. XDPB24), the National Key Research and Development Program of China (2020YFF0304600), the Program for Taishan Scholars of Shandong Province (no. ts20190965), the Innovation Leading Talents Program of Qingdao (19-3-2-23-zhc) in China, and the Fundamental Research Funds for the Central Universities (no. NE2019001) of China, a project funded by the Priority Academic Program Development of Jiangsu Higher Education Institutions.

AUTHOR CONTRIBUTIONS

D.W. and L.X. conceived the project idea, and L.Z. and L.J. carried out the experiments. H.C. and Y.G. did the theoretical calculation part. L.X., Y.Z., and Y.F. participated in the discussion of the article results. F.Z., W.L., W.G., and Z.L.W. supervised and coordinated the work. D.W. and Y.G. organized and wrote the manuscript with input from all authors. L.Z., L.X., D.W., and Z.L.W. revised the manuscript. All of the authors discussed the manuscript.

DECLARATION OF INTERESTS

The authors declare no competing interests.

Received: December 16, 2021
Revised: February 10, 2022
Accepted: February 19, 2022
Published: March 18, 2022

REFERENCES

1. Li, C., Liu, D., Xu, C., Wang, Z., Shu, S., Sun, Z., Tang, W., and Wang, Z.L. (2021). Sensing of joint and spinal bending or stretching via a retractable and wearable badge reel. Nat. Commun. *12*, 2950. https://doi.org/10.1038/s41467-021-23207-8.

2. Shao, J., Jiang, T., Tang, W., Xu, L., Kim, T.W., Wu, C., Chen, X., Chen, B., Xiao, T., and Bai, Y. (2018). Studying about applied force and the output performance of sliding-mode triboelectric nanogenerators. Nano Energy *48*, 292–300.

3. Wang, Z.L. (2019). Entropy theory of distributed energy for internet of things. Nano Energy *58*, 669–672. https://doi.org/10.1016/j.nanoen.2019.02.012.

4. Xu, W., Zheng, H., Liu, Y., Zhou, X., Zhang, C., Song, Y., Deng, X., Leung, M., Yang, Z., Xu, R.X., et al. (2020). A droplet-based electricity generator with high instantaneous power density. Nature *578*, 392–396. https://doi.org/10.1038/s41586-020-1985-6.

5. Zhao, Z., Zhou, L., Li, S., Liu, D., Li, Y., Gao, Y., Liu, Y., Dai, Y., Wang, J., and Wang, Z.L. (2021). Selection rules of triboelectric materials for direct-current triboelectric nanogenerator. Nat. Commun. *12*, 4686. https://doi.org/10.1038/s41467-021-25046-z.

6. Zhu, G., Pan, C., Guo, W., Chen, C.-Y., Zhou, Y., Yu, R., and Wang, Z.L. (2012). Triboelectric-generator-driven pulse electrodeposition for micropatterning. Nano Lett. *12*, 4960–4965.

7. Hua, Q., Sun, J., Liu, H., Bao, R., Yu, R., Zhai, J., Pan, C., and Wang, Z.L. (2018). Skin-inspired highly stretchable and conformable matrix networks for multifunctional sensing. Nat. Commun. *9*, 244. https://doi.org/10.1038/s41467-017-02685-9.

8. Kuang, S.Y., Zhu, G., and Wang, Z.L. (2018). Triboelectrification-enabled self-powered data storage. Adv. Sci. *5*, 1700658. https://doi.org/10.1002/advs.201700658.

9. Peng, X., Dong, K., Ye, C., Jiang, Y., Zhai, S., Cheng, R., Liu, D., Gao, X., Wang, J., and Wang, Z.L. (2020). A breathable, biodegradable, antibacterial, and self-powered electronic skin based on all-nanofiber triboelectric nanogenerators. Sci. Adv. *6*, eaba9624. https://doi.org/10.1126/sciadv.aba9624.

10. Wang, J., Wu, C., Dai, Y., Zhao, Z., Wang, A., Zhang, T., and Wang, Z.L. (2017). Achieving ultrahigh triboelectric charge density for efficient energy harvesting. Nat. Commun. *8*, 88. https://doi.org/10.1038/s41467-017-00131-4.

11. Wang, Z.L. (2017). New wave power. Nature *542*, 159–160. https://doi.org/10.1038/542159a.

12. Wu, Z., Cheng, T., and Wang, Z.L. (2020). Self-powered sensors and systems based on nanogenerators. Sensors *20*, 2925. https://doi.org/10.3390/s20102925.

13. Zhang, C., Chen, J., Xuan, W., Huang, S., You, B., Li, W., Sun, L., Jin, H., Wang, X., Dong, S., et al. (2020). Conjunction of triboelectric nanogenerator with induction coils as wireless power sources and self-powered wireless sensors. Nat. Commun. *11*, 58. https://doi.org/10.1038/s41467-019-13653-w.

14. Zhang, C., Guo, Z., Zheng, X., Zhao, X., Wang, H., Liang, F., Guan, S., Wang, Y., Zhao, Y., Chen, A., et al. (2020). A contact-sliding-triboelectrification-driven dynamic optical transmittance modulator for self-powered information covering and selective visualization. Adv. Mater. *32*, 1904988. https://doi.org/10.1002/adma.201904988.

15. Feng, Y., Zheng, Y., Zhang, G., Wang, D., Zhou, F., and Liu, W. (2017). A new protocol toward high output TENG with polyimide as charge storage layer. Nano Energy *38*, 467–476.

16. Lin, L., Wang, S., Niu, S., Liu, C., Xie, Y., and Wang, Z.L. (2014). Noncontact free-rotating disk triboelectric nanogenerator as a sustainable energy harvester and self-powered mechanical sensor. ACS Appl. Mater. Interfaces *6*, 3031–3038.

17. Lin, L., Xie, Y., Niu, S., Wang, S., Yang, P.-K., and Wang, Z.L. (2015). Robust triboelectric nanogenerator based on rolling electrification and electrostatic induction at an instantaneous energy conversion efficiency of~ 55%. ACS Nano *9*, 922–930.

18. Wang, P., Pan, L., Wang, J., Xu, M., Dai, G., Zou, H., Dong, K., and Wang, Z.L. (2018). An ultra-low-friction triboelectric–electromagnetic hybrid nanogenerator for rotation energy harvesting and self-powered wind speed sensor. ACS Nano *12*, 9433–9440.

19. Huang, X., Xiang, X., Nie, J., Peng, D., Yang, F., Wu, Z., Jiang, H., Xu, Z., and Zheng, Q. (2021). Microscale Schottky superlubric generator with high direct-current density and ultralong life. Nat. Commun. *12*, 2268. https://doi.org/10.1038/s41467-021-22371-1.

20. Berman, D., Deshmukh, S.A., Sankaranarayanan, S.K., Erdemir, A., and Sumant, A.V. (2015). Friction. Macroscale superlubricity enabled by graphene nanoscroll formation. Science *348*, 1118–1122. https://doi.org/10.1126/science.1262024.

21. Hod, O., Meyer, E., Zheng, Q., and Urbakh, M. (2018). Structural superlubricity and ultralow friction across the length scales. Nature *563*, 485–492. https://doi.org/10.1038/s41586-018-0704-z.

22. Huang, X., Lin, L., and Zheng, Q. (2020). Theoretical study of superlubric nanogenerators with superb performances. Nano Energy *70*, 104494. https://doi.org/10.1016/j.nanoen.2020.104494.

23. Li, R., Sun, C., Yang, X., Wang, Y., Gao, K., Zhang, J., and Li, J. (2022). Toward high load-bearing, ambient robust and macroscale structural superlubricity through contact stress dispersion. Chem. Eng. J. *431*, 133548. https://doi.org/10.1016/j.cej.2021.133548.

24. Li, R., Yang, X., Zhao, J., Yue, C., Wang, Y., Li, J., Meyer, E., Zhang, J., and Shi, Y. (2022). Operando formation of van der Waals heterostructures for achieving macroscale superlubricity on engineering rough and worn surfaces. Adv. Funct. Mater. 2111365. https://doi.org/10.1002/adfm.202111365.

25. Li, P., Ju, P., Ji, L., Li, H., Liu, X., Chen, L., Zhou, H., and Chen, J. (2020). Toward robust macroscale superlubricity on engineering steel substrate. Adv. Mater. *32*, 2002039. https://doi.org/10.1002/adma.202002039.

26. Erdemir, A. (2001). The role of hydrogen in tribological properties of diamond-like carbon films. Surf. Coat. Technol. *146*, 292–297. https://doi.org/10.1016/s0257-8972(01)01417-7.

27. Hauert, R. (2004). An overview on the tribological behavior of diamond-like carbon in technical and medical applications. Tribol. Int. *37*, 991–1003. https://doi.org/10.1016/j.triboint.2004.07.017.

28. Song, H., Ji, L., Li, H., Liu, X., Wang, W., Zhou, H., and Chen, J. (2016). External-field-induced growth effect of an a-C:H film for manipulating its medium-range nanostructures and properties. Acs Appl. Mater. Interfaces *8*, 6639–6645. https://doi.org/10.1021/acsami.5b11970.

29. Erdemir, A., Eryilmaz, O.L., and Fenske, G. (2000). Synthesis of diamondlike carbon films with superlow friction and wear properties. J. Vac. Sci. Technol. A *18*, 1987–1992. https://doi.org/10.1116/1.582459.

30. Angus, J.C. (1992). Diamond and diamond-like films. Thin Solid Films *216*, 126–133.

31. Jacob, W., and Moller, W. (1993). On the structure of thin hydrocarbon films. Appl. Phys. Lett. *63*, 1771–1773. https://doi.org/10.1063/1.110683.

32. Holmberg, K., Ronkainen, H., Laukkanen, A., and Wallin, K. (2007). Friction and wear of coated surfaces - scales, modelling and simulation of tribomechanisms. Surf. Coat. Technol. *202*, 1034–1049. https://doi.org/10.1016/j.surfcoat.2007.07.105.

33. Erdemir, A., Bindal, C., Fenske, G.R., Zuiker, C., and Wilbur, P. (1996). Characterization of transfer layers forming on surfaces sliding against diamond-like carbon. Surf. Coat. Technol. *86-7*, 692–697. https://doi.org/10.1016/s0257-8972(96)03073-3.

34. Ramaswamy, S.H., Shimizu, J., Chen, W., Kondo, R., and Choi, J. (2019). Investigation of diamond-like carbon films as a promising dielectric material for triboelectric nanogenerator. Nano Energy *60*, 875–885. https://doi.org/10.1016/j.nanoen.2019.03.095.

35. Zhang, W., Diao, D., Sun, K., Fan, X., and Wang, P. (2018). Study on friction-electrification coupling in sliding-mode triboelectric nanogenerator. Nano Energy *48*, 456–463. https://doi.org/10.1016/j.nanoen.2018.04.007.

36. Berman, D., Erdemir, A., and Sumant, A.V. (2018). Approaches for achieving superlubricity in two-dimensional materials. ACS Nano *12*, 2122–2137. https://doi.org/10.1021/acsnano.7b09046.

37. Martin, J.M., and Erdemir, A. (2018). SUPERLUBRICITY: friction's vanishing act. Phys. Today *71*, 40–46. https://doi.org/10.1063/pt.3.3897.

38. Irmer, G., and Dorner-Reisel, A. (2005). Micro-Raman studies on DLC coatings. Adv. Eng. Mater. *7*, 694–705. https://doi.org/10.1002/adem.200500006.

39. Liu, Y., Erdemir, A., and Meletis, E. (1996). A study of the wear mechanism of diamond-like carbon films. Surf. Coat. Technol. *82*, 48–56.

40. Liu, Y., and Meletis, E. (1997). Evidence of graphitization of diamond-like carbon films during sliding wear. J. Mater. Sci. *32*, 3491–3495.

41. Ma, T.-B., Hu, Y.-Z., Xu, L., Wang, L.-F., and Wang, H. (2011). Shear-induced lamellar ordering and interfacial sliding in amorphous carbon films: a superlow friction regime. Chem. Phys. Lett. *514*, 325–329.

42. Ma, T.-B., Wang, L.-F., Hu, Y.-Z., Li, X., and Wang, H. (2014). A shear localization mechanism for lubricity of amorphous carbon materials. Sci. Rep. *4*, 3662.

43. Song, H., Ji, L., Li, H., Liu, X., Zhou, H., Wang, W., and Chen, J. (2015). Perspectives of friction mechanism of aC: H film in vacuum concerning the onion-like carbon transformation at the sliding interface. RSC Adv. *5*, 8904–8911.

44. Li, S., Nie, J., Shi, Y., Tao, X., Wang, F., Tian, J., Lin, S., Chen, X., and Wang Zhong, L. (2020). Contributions of different functional groups to contact electrification of polymers. Adv. Mater. *32*, 2001307. https://doi.org/10.1002/adma.202001307.

45. Xu, C., Wang, A.C., Zou, H., Zhang, B., Zhang, C., Zi, Y., Pan, L., Wang, P., Feng, P., Lin, Z., and Wang, Z.L. (2018). Raising the working temperature of a triboelectric nanogenerator by quenching down electron thermionic emission in contact-electrification. Adv. Mater.

30, 1803968. https://doi.org/10.1002/adma.201803968.

46. Xu, C., Zi, Y., Wang, A.C., Zou, H., Dai, Y., He, X., Wang, P., Wang, Y.C., Feng, P., and Li, D. (2018). On the electron-transfer mechanism in the contact-electrification effect. Adv. Mater. *30*, 1706790.

47. Zhang, Z., Jiang, D., Zhao, J., Liu, G., Bu, T., Zhang, C., and Wang, Z.L. (2020). Tribovoltaic effect on metal–semiconductor interface for direct-current low-impedance triboelectric nanogenerators. Adv. Energy Mater. *10*, 1903713. https://doi.org/10.1002/aenm.201903713.

48. Liu, J., Liu, F., Bao, R., Jiang, K., Khan, F., Li, Z., Peng, H., Chen, J., Alodhayb, A., and Thundat, T. (2019). Scaled-up direct-current generation in MoS2 multilayer-based moving heterojunctions. Acs Appl. Mater. Interfaces *11*, 35404–35409. https://doi.org/10.1021/acsami.9b09851.

49. Wang, Z.L., and Wang, A.C. (2019). On the origin of contact-electrification. Mater. Today *30*, 34–51. https://doi.org/10.1016/j.mattod.2019.05.016.

50. Perdew, J.P., Burke, K., and Ernzerhof, M. (1996). Generalized gradient approximation made simple. Phys. Rev. Lett. *77*, 3865–3868. https://doi.org/10.1103/PhysRevLett.77.3865.

51. Kresse, G., and Furthmuller, J. (1996). Efficient iterative schemes for ab initio total-energy calculations using a plane-wave basis set. Phys. Rev. B *54*, 11169–11186. https://doi.org/10.1103/PhysRevB.54.11169.

52. Blöchl, P.E. (1994). Projector augmented-wave method. Phys. Rev. B *50*, 17953.

53. Klimeš, J., Bowler, D.R., and Michaelides, A. (2009). Chemical accuracy for the van der Waals density functional. J. Phys. Condens. Matter *22*, 022201.

54. Klimeš, J., Bowler, D.R., and Michaelides, A. (2011). Van der Waals density functionals applied to solids. Phys. Rev. B *83*, 195131.

55. Socoliuc, A., Bennewitz, R., Gnecco, E., and Meyer, E. (2004). Transition from stick-slip to continuous sliding in atomic friction: entering a new regime of ultralow friction. Phys. Rev. Lett. *92*, 134301. https://doi.org/10.1103/PhysRevLett.92.134301.

56. Medyanik, S.N., Liu, W.K., Sung, I.H., and Carpick, R.W. (2006). Predictions and observations of multiple slip modes in atomic-scale friction. Phys. Rev. Lett. *97*, 136106. https://doi.org/10.1103/PhysRevLett.97.136106.

57. Andersson, J., Erck, R.A., and Erdemir, A. (2003). Friction of diamond-like carbon films in different atmospheres. Wear *254*, 1070–1075. https://doi.org/10.1016/s0043-1648(03)00336-3.

58. Wang, Y., Li, H., Ji, L., Zhao, F., Liu, X., Kong, Q., Wang, Y., Quan, W., Zhou, H., and Chen, J. (2010). The effect of duty cycle on the microstructure and properties of graphite-like amorphous carbon films prepared by unbalanced magnetron sputtering. J. Phys. D Appl. Phys. *43*, 505401. https://doi.org/10.1088/0022-3727/43/50/505401.